RSC Advances

ROYAL SOCIETY OF CHEMISTRY

www.rsc.org/advances

Journal Name

RSCPublishing

ARTICLE

Hierarchical Structures of Olefinic Blocky Copolymer/Montmorillonite Nanocomposites with Collapsed and Intercalated Clay Layers

Cite this: DOI: 10.1039/x0xx00000x

Received 00th January 2014,
Accepted 00th January 2014

DOI: 10.1039/x0xx00000x

www.rsc.org/

Zai-Zai Tong, Bing Zhou, Jie Huang, Jun-Ting Xu,* Zhi-Qiang Fan

ABSTRACT: The hierarchical structures of olefinic blocky copolymer (OBC)/organically modified montmorillonite (OMMT) nanocomposites with different dispersion states of clay, including collapsed and intercalated OMMT (c-OMMT and i-OMMT), were characterized with various techniques. It is observed that, there are more densely stacked clay layers in single clay particles with a smaller size but larger distance between the adjacent clay particles in OBC/c-OMMT. c-OMMT exhibits stronger nucleation ability on crystallization of OBC than i-OMMT. This leads to a smaller size of the macroscopic crystals, thicker lamellar crystals, and more amorphous phase included into the inter-lamellae but less amorphous phase among different macroscopic crystals in OBC/c-OMMT. These differences in the hierarchical structure are responsible for the more obvious strain-hardening behavior but smaller strain at break of the OBC/c-OMMT nanocomposites.

1. Introduction

Olefinic blocky copolymers (OBCs) are a type of newly emerging thermoplastic elastomer synthesized by Dow Chemical.[1,2] OBCs have a multi-block structure, consisting of hard blocks with very low octene content and high melting temperature, and soft blocks with high octene content and almost no crystallinity.[3] OBCs can exhibit excellent mechanical properties and the structure-property relationship of OBCs has been well studied.[3-20] On the other hand, nanofillers with various shapes, such as nanospheres, nanotubes and nano-platelets, can be added into polymer matrixes to yield polymer nanocomposites and to improve and regulate the mechanical, thermal, and permeation properties of polymer materials. Nanoclay, which has a platelet shape with a nano-metric thickness, is frequently used as the nanofiller.[21-26] However, so far the OBC/clay nanocomposite has not been prepared by other groups previously.

The clay layers in the polymer matrix may exhibit different dispersion states, which greatly affect the properties of the nanocomposites. In literature, three different dispersion states have been reported: intercalation, exfoliation and aggregation, depending on the nature of the components used (layered silicate, modifier and polymer matrix) and the method of preparation. When the silicate layers are less affinitive to the polymer, aggregated structure tends to be formed.[27] In the intercalated structure the polymer chains are intercalated into the galleries of silicate layers. When each silicate layer is separated and uniformly dispersed in the continuous polymer matrix, an exfoliated structure is obtained.[23] Many researches have focused on the relationship of structure-property of the nanocomposites with different dispersion states of clay.[28-37] It is found that aggregated clay layers have limited improvement on the mechanical properties of the polymers.[28-30] By contrast, the intercalated or exfoliated clay layers can greatly improve the mechanical properties of polymers.[29-35] Moreover, we observed Regime III crystallization of polyethylene due to the confinement effect of the clay on the intercalated polymer chains.[36,37] Therefore, it is of great importance to investigate the clay dispersion and its effect on the properties of the nanocomposites.

Recently, we prepared the nanocomposites of OBC and organically modified montmorillonite with a severely collapsed clay structure (c-OMMT),[38] which is rarely reported in literature.[39-41] We found that the crystallization behavior and rheological property of the OBC/c-OMMT nanocomposites were quite different from those of the nanocomposites containing intercalated OMMT (i-OMMT) or aggregated un-modified MMT.[38] However, the structure of polymer nanocomposites containing collapsed clay layers has not been intensively characterized in literature, thus the properties of the OBC/c-OMMT nanocomposites have not been fully understood yet. In the present work, both OBC/c-OMMT and OBC/i-OMMT nanocomposites were prepared, and the structures at different scales, including nano- and micro-levels, were characterized using various techniques. This investigation will shed light on structure-property relationship of OBC/c-OMMT and OBC/i-OMMT nanocomposites.

MOE Key Laboratory of Macromolecular Synthesis and Functionalization, Department of Polymer Science & Engineering, Zhejiang University, Hangzhou 310027, China
**Correspondence author. E-mail: xujt@zju.edu.cn , Tel./Fax: +86-571-87952400*

2. Experimental section

Materials

The OBC pellets were kindly provided by Dow Chemical Company. The weight-average molecular mass and polydispersity (M_w/M_n) of OBC are 90 kg/mol and 3.1, respectively. The overall octene content in OBC is 13.2 mol%. The octene contents in the hard and soft blocks are 1.4 mol% and 23.7 mol%, respectively. The weight percentage of the hard block is 35.0%. The organically modified montmorillonite (OMMT, brand: Nanomer 1.44P) was purchased from Nonocor (USA). The OMMT was prepared through ion-exchange of MMT with dimethyl dehydrogenated tallow ammonium ions. The OMMT was dried under vacuum for 2 days at 50 °C prior to use.

Preparation of OBC/OMMT Nanocomposites

Details about preparation of two types of OBC/OMMT nanocomposites with different OMMT loadings were described in our previous work.[38] Firstly, the OBC was dissolved in xylene solution at 120 °C with a concentration of 1.0 w/v%. On the other hand, the OMMT was dispersed in xylene and sonicated for 60 min at room temperature. The OMMT/xylene mixture was slowly added into the OBC/xylene solution. After further stirring for 6 h, the hot solution was poured into excess ethanol, and OBC and OMMT were co-precipitated from the solution. The obtained nanocomposites have a collapsed clay structure. Such nanocomposites with different OMMT loadings are named as OBC/c-OMMT-*x*, where *x* represents the weight percentage of OMMT. By contrast, the nanocomposites having an intercalated clay structure with an OMMT loading of *x* wt% (named as OBC/i-OMMT-*x*) were prepared by directly evaporating the solvent, xylene, at 60 °C. The OMMT loadings in both OBC/c-OMMT and OBC/i-OMMT nanocomposites are 0.5, 1.0, 2.0, 3.0 wt%, respectively. The prepared nanocomposites were dried in vacuum for 2 days at 50 °C for further study.

Characterization

Differential scanning calorimetry. Specimens weighing 3-5 mg were cut from compression-molded films for thermal analysis. The differential scanning calorimetry (DSC) experiments were carried out on a TA Q200 calorimeter. The samples were firstly heated to 180 °C and held for 5 min to eliminate thermal history. Subsequently, the samples were cooled to 40 °C at a rate of 10 °C/min and the non-isothermal crystallization DSC curves were recorded. Finally the samples were again heated to 180 °C at a rate of 10 °C/min to obtain the melting curves. The temperature was calibrated with indium.

Wide angel X-ray diffraction. Samples for room temperature wide angle X-ray diffraction (WAXD) were cut from compression-molded films (~0.2 mm thickness). The WAXD experiments were performed at BL14B beamline in Shanghai Synchrotron Radiation Facility (SSRF) in China. The wavelength of the X-ray source was 1.24 Å. The range of diffraction angle for investigation was 2θ=1-26° and the scanning step is 0.02°. The basal spacing of the clay layer (d_{001}) was calculated using the Bragg's equation: $d_{001}=\lambda/(2\sin\theta)$. The mean clay size, D_{clay}, in the direction perpendicular to the (001) plane was calculated from the Scherrer equation:[42]

$$D_{clay} = \frac{K\lambda}{\beta \cos\theta_{001}} \quad (1)$$

Where K is the shape factor (usually 0.89), λ is the wavelength of X-ray, β is the value of the full width at half maximum (FWHM), and θ_{001} is the Bragg angle at (001) plane. The parameter D_{clay} can be viewed as the thickness of clay stack perpendicular to the (001) plane, the number of platelets per clay particle, N, can be calculated with as follows:[43]

$$N = \frac{D_{clay} - d_p}{d_{001}} + 1 \quad (2)$$

Where d_p is the thickness of one single platelet with a value of ~1.0 nm.

Diffraction peaks from OBC can be detected by WAXD as well at larger diffraction angles. The WAXD profiles can be deconvolved into three peaks: two crystalline peaks and one amorphous halo by fitting the curves with multiple Gaussian functions. The weight fraction crystallinity of OBC is calculated based on the following equation:

$$X_c^{WAXD} = \frac{A_c}{A_c + A_a} \times 100\% \quad (3)$$

Where A_c is the total area of the crystalline peaks, and A_a is the area of the amorphous halo.

Transmission electron microscopy. Morphology of the OBC/clay nanocomposites was observed by transmission electron microscopy (TEM) on a JEOL JEM-1200EX instrument at an acceleration voltage of 90 kV. The ultrathin films for TEM observation were prepared from the compression-molded films at -80 °C on a microtome machine.

Small angle X-ray scattering. Small angle X-ray scattering (SAXS) experiments were performed at BL16B1 beamline in Shanghai Synchrotron Radiation Facility (SSRF) in China. The wavelength of X-ray was 1.24 Å and the sample-to-detector distance was set as 5100 mm. Two-dimensional (2D) SAXS patterns at room temperatures were recorded. The average exposure time was 300 s for each scan. Bull tendon was used as standard material for calibrating the scattering vector. The 2D SAXS patterns were converted into one-dimensional (1D) SAXS profiles using Fit2D software.

The structural parameters describing the lamellar stacking of OBC crystals were derived from normalized one-dimensional correlation function, which is obtained through Fourier transformation of the Lorentz-corrected SAXS profile based on following equation:[44-46]

$$\gamma(r) = \frac{\int_0^\infty I(q) q^2 \cos(qr) dq}{\int_0^\infty I(q) q^2 dq} \quad (4)$$

Where $I(q)$ is the scattering intensity, q is the scattering vector defined as $q=4\pi\sin\theta/\lambda$, and λ is the X-ray wavelength. The details of this method have been reported in our previous works.[17,18] Useful structural parameters such as lamellar thickness l_c, long period L and amorphous layer ($l_a=L-l_c$) can been obtained from the curve of correlation function. The linear crystallinity X_l is governed by l_c and L, which is defined as:

$$X_l = \frac{l_c}{L} \quad (5)$$

On the other hand, the bulk volume fraction crystallinity, X_{vol}, can be calculated from the weight fraction crystallinity measured from WAXD (X_c^{WAXD}):

$$X_{vol} = \frac{\rho_a}{\rho_c / X_c^{WAXD} - \rho_c + \rho_a} \quad (6)$$

Where ρ_c and ρ_a are the densities of the crystalline and amorphous phases (for PE, ρ_c=1.000 g/cm^3 and ρ_a=0.855 g/cm^3)[3], respectively. The volume fraction crystallinity is also the product of linear crystallinity and the volume fraction of the lamellar stacks in the sample, Φ_s:

$$\Phi_s = \frac{X_{vol}}{X_l} \quad (7)$$

Φ_s can serve as a measurement for the extent of inter-lamellar segregation.[47,48]

Polarized optical microscopy. Polarized optical microscopy (POM) observations were carried out on an Olympus microscope (BX51) equipped with a hot stage. Thin film specimens of about 0.05 mm thickness were used for observation.

Mechanical property. The stress-strain behavior under uniaxial tension was performed on a CMT 4204 instrument. The tensile specimens were cut from the compression molded films with the thickness of about 0.5 mm. The distance of two grips was 15 mm and the specimen width was 7.2 mm. A strain rate of 30 mm/min was applied to uniaxial tension. Due to the limited quantity of the samples, the tests were repeated three times for each sample and the averaged data were reported.

3. Results and discussion

3.1. Structure and Dispersion State of Clay The WAXD patterns of OBC/c-OMMT and OBC/i-OMMT with various OMMT loadings are shown in Fig. 1. WAXD was done at small angles to determine the dispersion state of clay and at wide angles to characterize the crystalline phase of OBC. The basal reflection of the clay in the OBC/c-OMMT nanocomposites appears at a much larger angle, as compared with that of the neat OMMT. The calculated d-spacing of the (001) basal refection is 1.42 nm for the OBC/c-OMMT nanocomposites, whereas it is 2.67 nm for the neat OMMT and 3.88 nm for the OBC/i-OMMT nanocomposites. This indicates a severely collapsed structure of the clay layers in OBC/c-OMMT, but an intercalated structure in OBC/i-OMMT. Our previous work revealed that parts of the organic modifiers in the clay galleries were extracted by the solvent ethanol.[38] Collapse of the clay layers may occur due to the ambient pressure produced by solvent evaporation or melt-blending during preparation of the OBC/c-OMMT nanocomposites. It is also observed that the loading of OMMT has no significant influence on the value of d_{001} for two types of nanocomposites, with only the exception of the OBC/c-OMMT-0.5 sample, which has a smaller d_{001} than other OBC/c-OMMT nanocomposites.

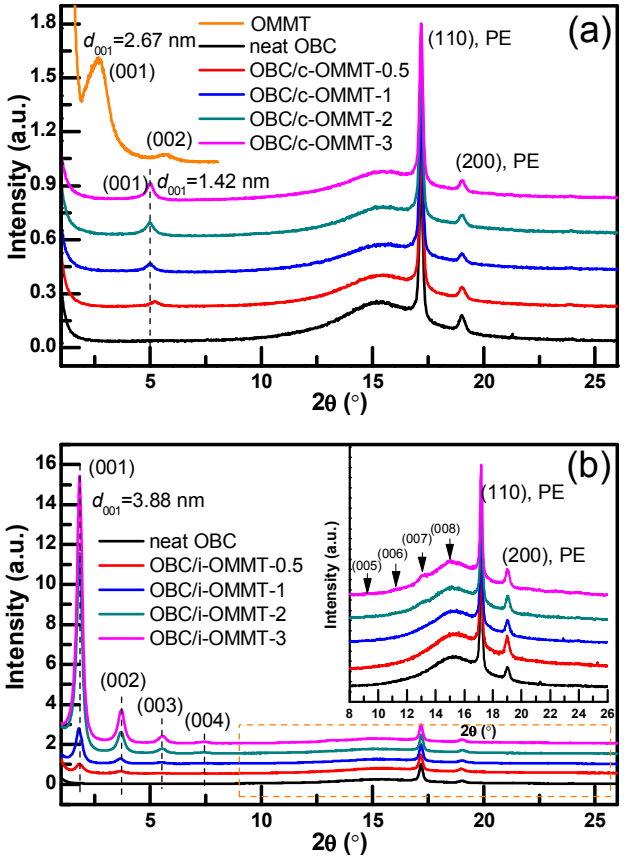

Fig. 1 WAXD patterns of OBC/c-OMMT nanocomposites (a), and OBC/i-OMMT nanocomposites (b) with different OMMT loadings. Inset shows the enlarged zone in the dashed box. For comparison, the WAXD patterns of neat OMMT and neat OBC are included. The curves are vertically offset for clarity.

Interestingly, when comparing the diffraction intensities of c-OMMT and i-OMMT at low angles, the (001) diffraction intensities of i-OMMT and c-OMMT, are remarkably different, especially at the clay loadings of 2.0 and 3.0 wt%. Since the OBC contents in the nanocomposites are similar and the OBCs have similar crystallinity, the (110) peak intensity of the orthorhombic PE crystal at 2θ=17.2° can be used as a reference. The (001) diffraction intensity of c-OMMT is evidently weaker than that of the (110) peak of PE (Fig. 1a), whereas the (001) diffraction intensity of i-OMMT is much stronger than that of the (110) peak of PE (Fig. 1b). Due to the high diffraction intensities of i-OMMT, the high order diffraction peaks of i-OMMT can even be discernible, as indicated in Fig. 1b. This striking difference in diffraction intensity at the same clay

loading also results from the different structures of the clay in the polymer matrix. It is known the diffraction intensity is proportional to the square electron density difference between two phases, $(\Delta\rho)^2$. In this case, two phases in the clay stacks are the silicate layer with a very high electron density and the organic modifiers in the clay galleries with a low electron density. When the distance of the clay galleries is changed, the electron density of modifier phase varies accordingly. Therefore, the value of $(\Delta\rho)^2$ is largely dependent on the distance of the clay galleries. In i-OMMT, the distance of clay galleries is increased to 2.88 nm (d_{001}-1, the thickness of silicate layer is usually around 1.0 nm). On the other hand, the distance in c-OMMT is decreased to 0.42 nm, which means that the electron density of modifier phases in c-OMMT is 6.8 times larger than that in i-OMMT. This suggests the value of $(\Delta\rho)^2$ in i-OMMT is much larger than that in c-OMMT, thus i-OMMT exhibits much stronger diffraction intensity than c-OMMT. This observation further confirms the different structures of the clay in these two types of nanocomposite.

The dispersion state of the clay is further quantitatively discussed by analysis of the WAXD profiles. The mean clay size, D_{clay}, in the direction perpendicular to the (001) plane of clay, which is related to the thickness of the clay layer stacks, is calculated based on Eq 1. The number of the platelet in per clay particle, N, is estimated according to Eq 2. The obtained data of D_{clay} and N are summarized in Table 1. The parameter D_{clay} gradually increases with the clay loading in both the OBC/c-OMMT and OBC/i-OMMT nanocomposites (Table 1). We also notice that D_{clay} of i-OMMT is much larger than that of c-OMMT at the same clay loading (Table 1). This is mainly due to the larger d_{001} of i-OMMT (3.88 nm) than that of c-OMMT (1.42 nm). The estimated value of N is about 8-10 for c-OMMT, which is larger than the value of 5-7 for i-OMMT. This shows that the clay layers are more easily separated in the OBC/i-OMMT nanocomposites due to intercalation of the polymer chains. By contrast, more clay layers stacks together in the OBC/c-OMMT nanocomposites because of the compression effect exerted by the OBC matrix.

Table 1 Characteristic parameters of two types of nanocomposites

Sample name	d_{001} (nm)	D_{clay} (nm)	N	S_{clay} (nm)	ζ_{clay} (nm)	X_c^{WAXD} (%)
neat OBC	-	-	-	-	-	16.0
OBC/c-OMMT-0.5	1.36	11.0	8.4	150	530	19.0
OBC/c-OMMT-1	1.42	12.7	9.2	250	480	19.4
OBC/c-OMMT-2	1.42	13.0	9.5	320	380	20.0
OBC/c-OMMT-3	1.42	13.3	9.7	360	250	20.0
OBC/i-OMMT-0.5	3.88	17.0	5.1	150	440	14.4
OBC/i-OMMT-1	3.88	19.8	5.9	260	360	15.3
OBC/i-OMMT-2	3.83	22.3	6.6	340	280	15.6
OBC/i-OMMT-3	3.84	23.6	6.9	380	160	14.6

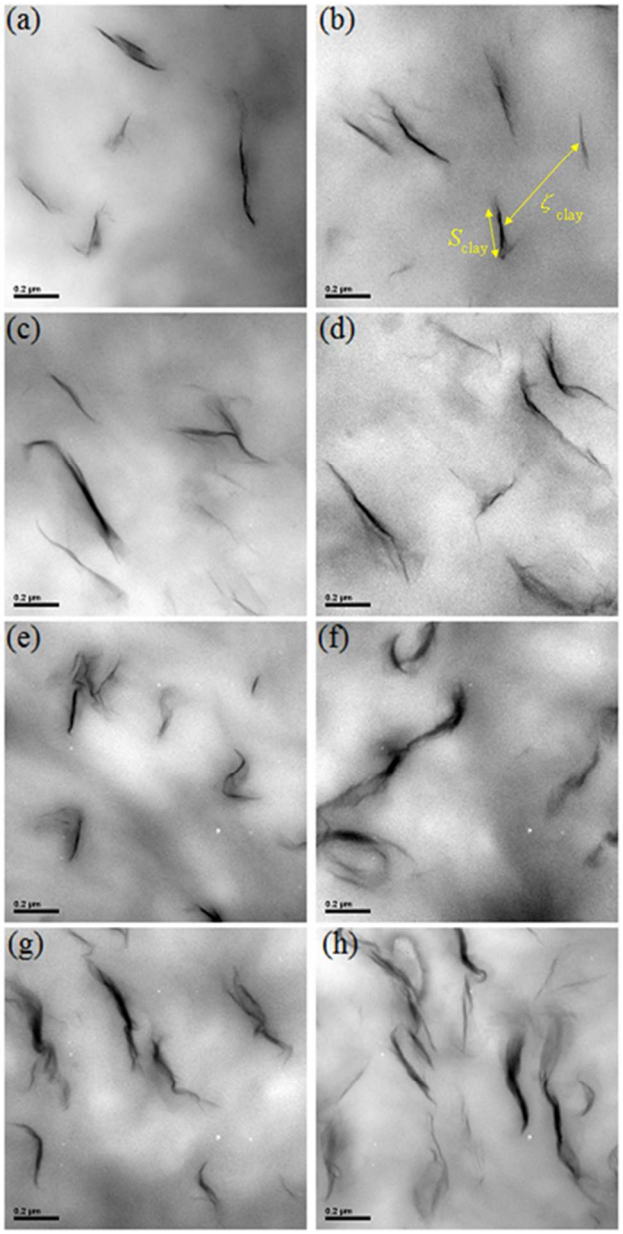

Fig. 2 TEM images of different OBC/OMMT nanocomposites with various OMMT loading. OBC/c-OMMT-0.5 (a), OBC/c-OMMT-1 (b), OBC/c-OMMT-2 (c), OBC/c-OMMT-3 (d), OBC/i-OMMT-0.5 (e), OBC/i-OMMT-1 (f), OBC/i-OMMT-2 (g) and OBC/i-OMMT-3 (h). The scale bar in the figure is 200 nm.

The morphology of the OBC/c-OMMT and OBC/i-OMMT nanocomposites was also characterized with TEM, as shown in Fig. 2. In each nanocomposite, the clay stacks are well and randomly dispersed in the OBC matrix. With increasing in the OMMT loading, more flocculated OMMT layers are observed. This is in accordance with the larger value of D_{clay} at high OMMT loading calculated from WAXD result. The statistical length of clay (S_{clay}) and the statistical correlation between the dispersed layers (ζ_{clay}) were obtained from the TEM micrographs. S_{clay} represents the lateral size of the clay stacks

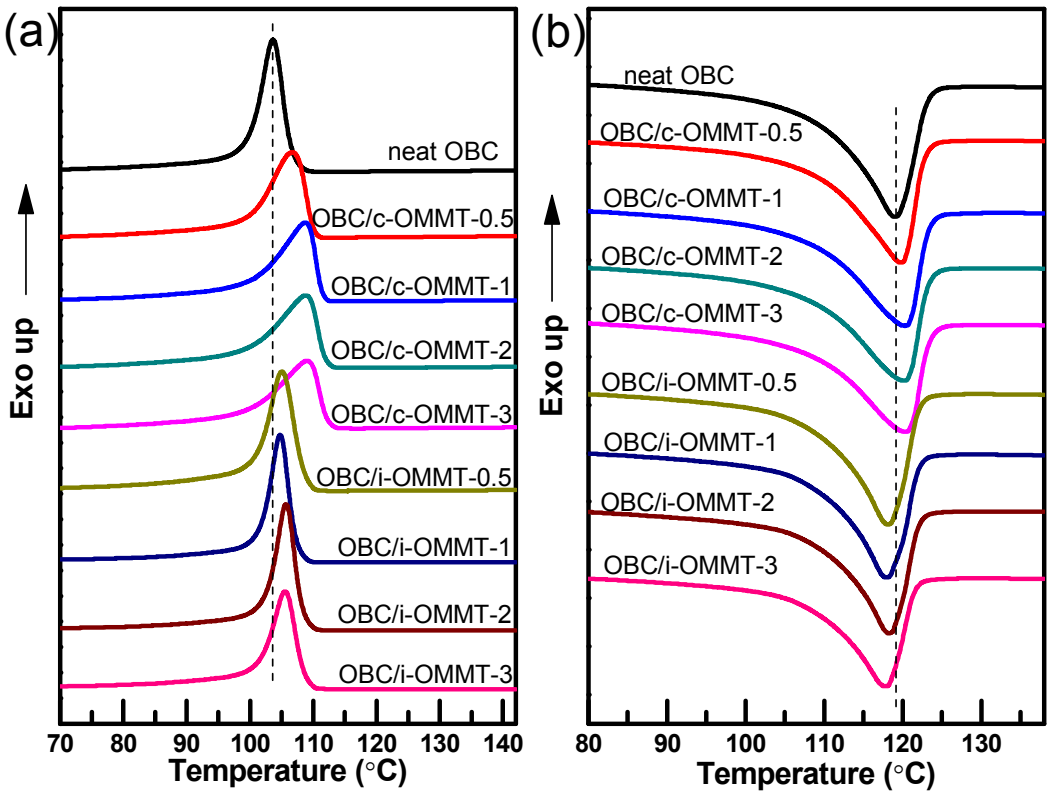

Fig. 3 DSC traces of non-isothermal crystallization (a) and subsequent melting (b) for neat OBC and all the nanocomposites. Both the cooling and heating rate is 10 ℃/min. The curves are vertically offset for clarity.

and ζ_{clay} stands for the mean distances between the adjacent clay stacks, as shown in Fig. 2b. The values of S_{clay} and ζ_{clay} are listed in Table 1. As the clay loading increases, S_{caly} increase from ~150 nm to ~360 nm for both c-OMMT and i-OMMT. The increase of the lateral size of clay is owing to the higher probability of hydroxylated edge-edge interaction between different clay layers at a higher clay loading. On the other hand, the values of ζ_{clay} for both c-OMMT and i-OMMT decrease with the clay loading (Table 1). This is understandable, since the mean distance between the adjacent clay stacks will decreases as the clay loading becomes higher. Moreover, ζ_{clay} of i-OMMT is always smaller than that of c-OMMT at the same clay loading. Such a result is quite normal. The clay layers in c-OMMT are collapsed, while they are intercalated in i-OMMT. Calculation based on the data of d_{001} shows that the volume fraction of i-OMMT is about 1.7 times larger than that of c-OMMT in the nanocomposites with the same clay loading.

The WAXD and TEM analyses show that the structure and dispersion states of the clay particles are quite different in the OBC/c-OMMT and OBC/i-OMMT nanocomposites. The clay layers are densely stacked with more layers in per clay particle and a larger mean distance between the adjacent clay particles in the OBC/c-OMMT nanocomposites. By contrast, the clay layers are loosely stacked in the OBC/i-OMMT nanocomposites due to intercalation of OBC chains, leading to fewer layers in per clay particle and a smaller mean distance between the adjacent clay particles. Such a difference can account for the different rheological behaviors of the melts of the OBC/c-OMMT and OBC/i-OMMT nanocomposites. We observed that the OBC/c-OMMT nanocomposites exhibit smaller storage and loss moduli, and thus lower complex viscosity, than the OBC/i-OMMT nanocomposites at lower shear frequencies.[38] This can be ascribed to the collapsed structure and thus lower volume fraction of c-OMMT in OBC/c-OMMT nanocomposites. On the other hand, the complex viscosity of the OBC/i-OMMT nanocomposites at larger shear frequencies is smaller than that of the OBC/c-OMMT nanocomposites. This is due to intercalation of OBC chains into the galleries of i-OMMT, which drives the orientation of the clay particles more easily, leading to smaller complex viscosity and a more pronounced shear-thinning effect of the OBC/i-OMMT nanocomposites.

3.2. Thermal Behavior Fig. 3 shows the DSC cooling and subsequent heating curves of the neat OBC and both types of nanocomposite at various clay contents. The data of crystallization peak temperatures (T_c^p), onset crystallization temperatures (T_c^{onset}), melting temperatures (T_m), melting enthalpy (ΔH_m), and crystallinity (X_c^{DSC}) are summarized in Table 2. It is found that both OBC/c-OMMT and OBC/i-OMMT nanocomposites have higher T_c^p and T_c^{onset} than the neat OBC, showing that both c-OMMT and i-OMMT can nucleate polymer crystallization, like other nanofillers.[49,50] However, we notice that the T_c^p and T_c^{onset} of OBC/c-OMMT are always larger than those of OBC/i-OMMT with the same

Table 2 Thermal properties and crystallinity of the nanocomposites

Sample name	T_c^p (°C)	T_c^{onset} (°C)	T_m (°C)	ΔH_m (J/g)	$X_c^{DSC\,a}$
neat OBC	103.6	109.1	119.2	43.5	15.0%
OBC/c-OMMT-0.5	106.7	111.1	119.7	44.0	15.2%
OBC/c-OMMT-1	108.8	112.4	120.1	43.6	15.0%
OBC/c-OMMT-2	109.1	113.2	120.3	44.6	15.4%
OBC/c-OMMT-3	109.3	113.8	120.6	43.8	15.1%
OBC/i-OMMT-0.5	105.0	110.8	118.1	40.6	14.0%
OBC/i-OMMT-1	104.7	109.4	118.0	41.2	14.2%
OBC/i-OMMT-2	105.7	110.6	118.2	42.7	14.7%
OBC/i-OMMT-3	105.5	111.1	117.8	35.6	12.3%

[a] $X_c=\Delta H_m/\Delta H_m^0$, where ΔH_m^0 is the fusion enthalpy of the PE crystal of 100 % crystallinity (ΔH_m^0=290 J/g).

OMMT content. This indicates that c-OMMT has a stronger nucleation effect on crystallization of OBC than i-OMMT, which has been reported in our previous work.[38] Herein we focus on the effect of clay loading on the crystallization and melting behaviors. For the OBC/c-OMMT nanocomposites, the T_c^p increases from 106.7 °C of OBC/c-OMMT-0.5 to 109.3 °C of OBC/c-OMMT-3. Although the T_c^p is almost unchanged after the clay content reaches 1.0 wt%, the T_c^{onset} still increases with the OMMT loading (Table 2). In other words, T_c^{onset} is more sensitive to c-OMMT content than the T_c^p. Possible explanation is that T_c^{onset} is more closely related to the nucleation process during the initial crystallization period. This shows that, the higher the c-OMMT content, the stronger the nucleation effect. However, such a tendency is not observed for the OBC/i-OMMT nanocomposites. The i-OMMT content has no significant effect on T_c^p and T_c^{onset}, though the OBC/i-OMMT nanocomposites exhibit higher T_c^p and T_c^{onset} than the neat OBC. As pointed out above, T_c^{onset} is more related to the nucleation process in the initial crystallization period. Therefore, more nucleation sites can be provided at a higher clay loading. However, in the OBC/i-OMMT nanocomposites parts of polymer segments are confined in the clay galleries due to intercalation. At the same time, parts of these intercalated polymer chains are also located nearby the outer surface of i-OMMT particles, which may hinder nucleation of OBC on the clay surfaces and retard crystallization. Such a phenomenon is frequently reported in the nanocomposites of semicrystalline polymers with an intercalated clay structure.[36,37,51-53] Co-existence of confinement and nucleation effects of i-OMMT leads to the irregular and limited change of T_c^p and T_c^{onset} with the i-OMMT loading for the OBC/i-OMMT nanocomposites. By contrast, few polymer chains are confined in the OBC/c-OMMT nanocomposites, thus both T_c^p and T_c^{onset} monotonously increase with the c-OMMT loading.

It is observed that T_m of the OBC/c-OMMT nanocomposites slightly increases with the c-OMMT loading. The OBC/c-OMMT nanocomposites have similar crystallinity with the neat OBC (Table 2). By contrast, the T_ms and crystallinity of the OBC/i-OMMT nanocomposites are smaller than those of the neat OBC, though the T_c^ps of the OBC/i-OMMT nanocomposites are larger than that of the neat OBC (Table 2). It is known that melting temperature of polymer crystals is dependent on the thickness of crystal lamellae.[54] The higher T_m indicates that more perfect OBC crystals are formed in the presence of c-OMMT, which will be further discussed in terms of the lamellar crystal thickness in the next section. On the other hand, for OBC/i-OMMT nanocomposites, both the lower T_m and crystallinity reflect a confinement effect of i-OMMT towards crystallization of OBC, which is mainly due to the intercalation of polymer chains into the clay galleries, as mentioned above.

3.3. Crystal Structure of OBC WAXD was also applied to characterize the crystal structure of OBC. The room temperature WAXD patterns in the range of 2θ=8-26º, in which the reflections of the OBC crystals appear, are shown in Fig. 1. All the curves show three typical diffraction peaks of polyethylene (PE). The broad diffraction peak at 2θ=15.3º is assigned to the amorphous halo, which is formed by the soft blocks as well as the non-crystalline part of the hard blocks in the OBC. The two sharp diffraction peaks at 2θ of 17.2° and 19.0° correspond to the (110) and (200) reflections of orthorhombic PE crystal, respectively. Although different amounts of clay is blended with OBC, both c-OMMT and i-OMMT have no profound effect on the crystal structure, as indicated by the invariant peak positions of both (110) and (200) planes. Moreover, the weight fraction crystallinity (X_c^{WAXD}) is calculated according to Eq 3, and the data of X_c^{WAXD} are listed in Table 1. It is observed that X_c^{WAXD} of all the OBC/c-OMMT samples is larger than that of the neat OBC, while X_c^{WAXD} of the OBC/i-OMMT samples is slightly smaller than that of the neat OBC.

3.4. Lamellar Structure of OBC Crystals The stacking of polymer lamellae at tens of nanometer in the nanocomposites was characterized with SAXS. Fig. 4 shows the Lorentz-corrected SAXS profiles obtained at room temperature for both types of nanocomposite and the neat OBC. The long period L^* of different samples can be calculated from q_{max} by $L^*=2\pi/q_{max}$, where q_{max} is the peak position in the SAXS profiles. The SAXS profiles of the nanocomposites can be further analyzed with one-dimensional correlation function, as shown in Fig. 5. Some useful structural parameters, including lamellar thickness (l_c), amorphous layer (l_a), long period (L) and linear crystallinity (X_l), can be derived from the one-dimensional correlation function. Two values reflecting the thicknesses of the amorphous and crystalline layers are obtained from the one-dimensional correlation function. Because the crystallinity of OBC is less than 0.5, we assign the smaller value to l_c and the large one to l_a. The obtained structural parameters are shown in Fig. 6 and Table 3. It is found that the long periods derived from the correlation function (L) are quite similar to those calculated from the Brag equation (L^*) (Table 3). Moreover, for the OBC/c-OMMT samples, L gradually increases with the c-OMMT content. The value of L for OBC/c-OMMT-3 is up to 39.2 nm, which is 10.3 nm larger than that of the neat OBC. On

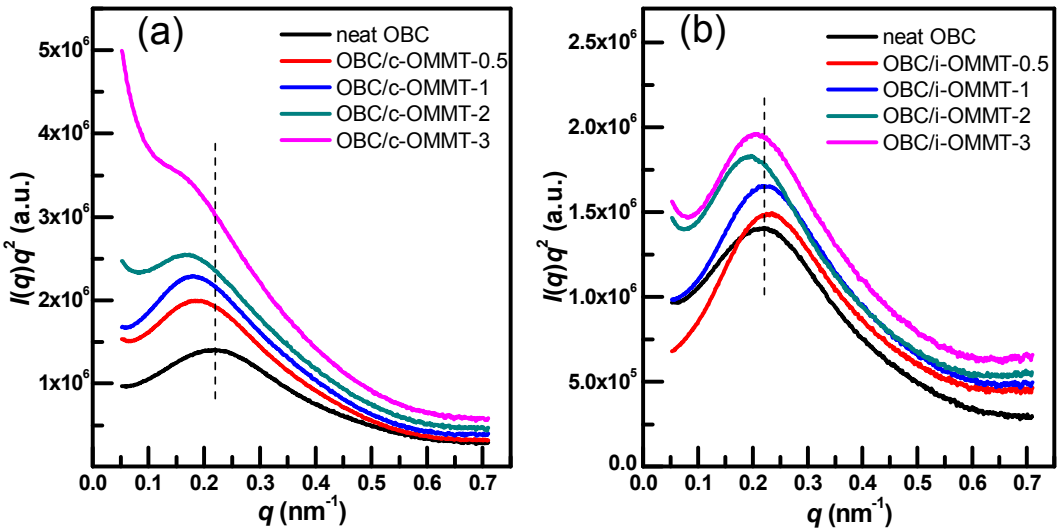

Fig. 4 Lorentz corrected profiles of OBC/c-OMMT nanocomposites (a) and OBC/i-OMMT nanocomposites (b) with various OMMT loading. The data of the neat OBC are also presented for comparison.

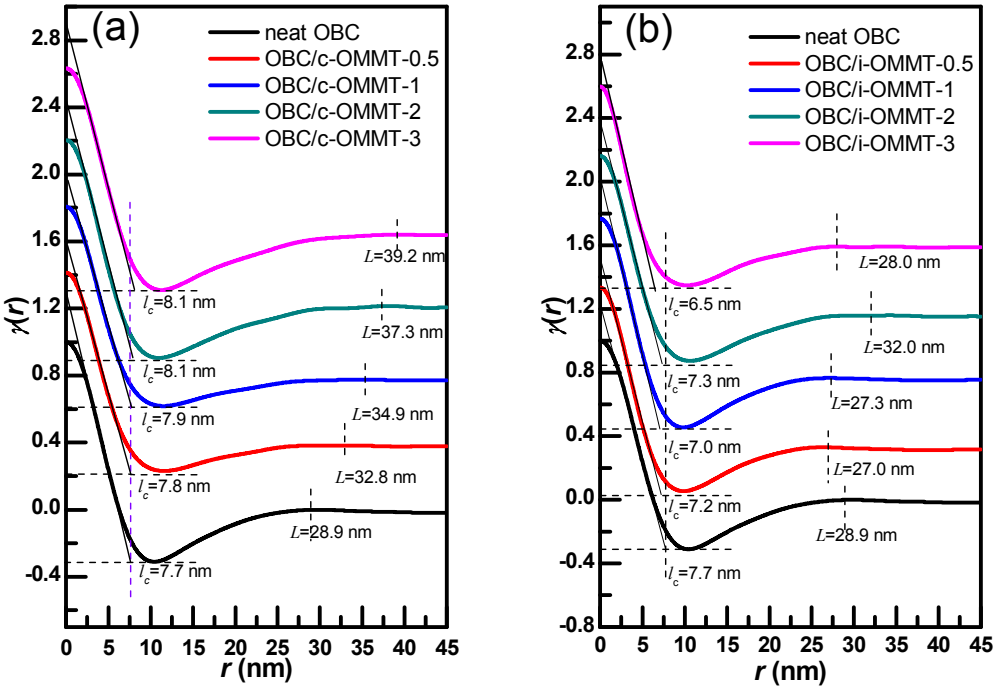

Fig. 5 One-dimensional correlation functions for OBC/c-OMMT nanocomposites (a) and OBC/i-OMMT nanocomposites (b). The data of l_c and L are indicated. The curves are vertically offset for clarity.

the other hand, the long period of the OBC/i-OMMT samples first increases as the i-OMMT content increases, and reach a maximum at the i-OMMT loading of 2.0 wt%, then decreases with further increase of the i-OMMT loading. Compared with the long periods of the OBC/c-OMMT samples, the long periods of the OBC/i-OMMT nanocomposites are evidently smaller.

It is found that l_c of the OBC/c-OMMT samples is slightly larger than that of the neat OBC, but the OBC/i-OMMT nanocomposites have a smaller l_c than the neat OBC. Since l_c is related to the melting temperature, there is good agreement between the lamellar thicknesses calculated from SAXS and the melting temperatures measured from DSC. This verifies that c-OMMT induces formation of thicker crystals, which can be attributed to the nucleation effect of c-OMMT and thus higher crystallization temperature. By contrast, i-OMMT leads to formation of thinner crystals because of the lower mobility of the OBC chains due to intercalation and lower crystallization temperature. On the other hand, the value of l_a for the OBC/c

Table 3 Structural Parameters of the Samples Obtained From One-Dimensional Correlation Functions of SAXS

Sample name	l_c (nm)	l_a (nm)	L (nm)	L^* [a] (nm)	X_l	X_{vol}	Φ_s
neat OBC	7.7	21.2	28.9	28.7	0.266	0.140	52.6%
OBC/c-OMMT-0.5	7.8	25.0	32.8	32.7	0.238	0.167	70.2%
OBC/c-OMMT-1	7.9	27.0	34.9	34.3	0.226	0.171	75.7%
OBC/c-OMMT-2	8.1	29.2	37.3	37.2	0.217	0.176	81.1%
OBC/c-OMMT-3	8.1	31.1	39.2	39.2	0.207	0.176	85.0%
OBC/i-OMMT-0.5	7.2	19.8	27.0	27.0	0.267	0.126	47.2%
OBC/i-OMMT-1	7.0	20.9	27.3	27.9	0.251	0.134	53.4%
OBC/i-OMMT-2	7.3	24.7	32.0	32.2	0.228	0.136	59.6%
OBC/i-OMMT-3	6.5	21.6	28.0	30.5	0.232	0.128	55.2%

[a] Obtained from Bragg's equation.

OMMT samples is evidently larger than that for the OBC/i-OMMT samples at the same OMMT loading.

The linear crystallinity, X_l, can be obtained based on Eq 5. Compared with the bulk volume crystallinity (X_{vol}) calculated in terms of Eq 6 (Table 3), X_l is always larger than X_{vol}. From the ratio of X_{vol} over X_l, the volume fraction of lamellar stacks in the samples, Φ_s, can be estimated (Eq 7). As shown in Table 3, the value of Φ_s for the neat OBC is only 0.526, which indicates that a large amount of amorphous phase is expelled out of the inter-lamellar stacks. By contrast, in the presence of c-OMMT, there is an obvious increase of Φ_s with the clay loading. This shows that more and more amorphous phase is included into inter-lamellae as the c-OMMT content increases, leading to expansion of the amorphous layer and thus a larger L. The difference in the amount of the amorphous phase included into inter-lamellae can be interpreted in terms of the different nucleation abilities of c-OMMT and i-OMMT. It has been reported that crystalline lamellae are preferential in the proximity of the clay platelets, which is a consequence of nucleation.[55-60] Therefore OMMT platelets are directly surrounded by the OBC lamellae, and the lamellar crystals are always approximately perpendicular to the OMMT surface. The surface area is one of the factors affecting the nucleation ability of nanofillers. Based on the number of the platelet in per clay particle (Table 1), it is estimated that the outer surface area of i-OMMT in OBC/i-OMMT should be about 1.5 times that of c-OMMT in OBC/c-OMMT. As a result, the weaker nucleation ability of i-OMMT cannot be attributed to the larger size of the i-OMMT particles, but to the interference effect of the intercalated polymer chains on nucleation. The chain segments located outside the i-OMMT galleries, which are chemically linked to the intercalated chain segments, may hinder nucleation of other OBC chains on the i-OMMT surface, leading to a lower nucleus density on the surface of i-OMMT. Since there are more crystal nuclei in the OMMT/c-OMMT nanocomposites, most of the polymer chains are nearby the nuclei and the amorphous phase can be easily included into the inter-lamellae during crystal growth. On the other hand, there are lots of polymer chains far from the nuclei in the OMMT/i-OMMT nanocomposites due to a lower nucleus density, thus a larger amount of the amorphous phase is left outside the inter-lamellae when the crystallizable chains diffuse to the lamellar crystal during crystal growth.

3.5. Macroscopic Morphology Fig. 7 shows the POM morphologies of two types of nanocomposite at various OMMT contents, after cooling from 180 °C at a rate of 10 °C/min. The morphologies of neat OBC, OBC/c-OMMT-3, and OBC/i-OMMT-3 are reported in previous work.[38] As the c-OMMT content increases, the morphology of OBC/c-OMMT nanocomposites changes dramatically. A larger number of spherulites with a smaller size are weakly discernible in OBC/c-OMMT-0.5, as compared with those in the neat OBC. When the c-OMMT content reaches 1.0 wt% or higher, only tiny crystallites instead of spherulites with abundant nucleation sites are observed, as shown in Fig. 7a-7c. This is well consistent with stronger nucleation ability of c-OMMT. The decreased crystallite size and increased crystallite number are frequently reported for the semicrystalline polymer/clay nanocomposites.[61] On the other hand, all the OBC/i-OMMT nanocomposites exhibit spherulite morphology. The spherulite

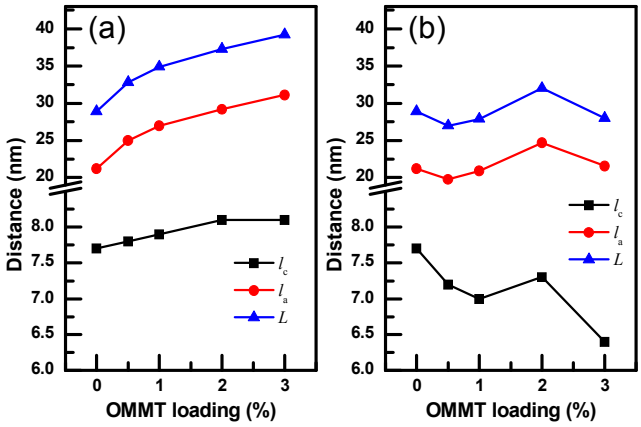

Fig. 6 Variations of the crystal layer thickness (l_c), amorphous layer thickness (l_a) and long period (L) with the OMMT loading for OBC/c-OMMT (a) and OBC/i-OMMT (b).

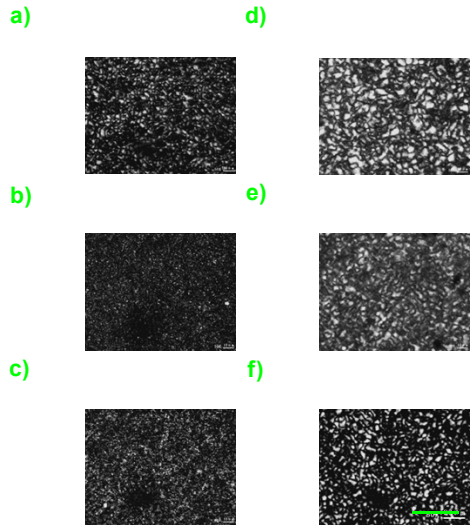

Fig. 7 POM images of the nanocomposites with various OMMT loading after cooling from 180 °C to room temperature at a rate of 10 °C /min. OBC/c-OMMT-0.5 (a), OBC/c-OMMT-1 (b), OBC/c-OMMT-2 (c), OBC/i-OMMT-0.5 (d), OBC/i-OMMT-1 (e) and OBC/i-OMMT-2 (f). The scale bar in the figure is 40 μm.

size decreases slightly with increasing of the i-OMMT content (Fig. 7d-7f). This shows that the morphology of the OBC/i-OMMT nanocomposites is less sensitive to the i-OMMT content, which is in accordance with the weaker nucleation ability of i-OMMT.In combination with all the results obtained from various characterization techniques, the hierarchical structures of two types of nanocomposite from nano- to micro-levels can be established, as schematically illustrated in Scheme 1. More clay layers are densely stacked with a longer distance between adjacent clay particles but a smaller volume fraction of clay in OBC/c-OMMT nanocomposites. The strong nucleation ability of c-OMMT leads to the smaller size of the macroscopic crystals, the thicker lamellae and more amorphous phase included into the inter-lamellae in the OBC/c-OMMT nanocomposites.

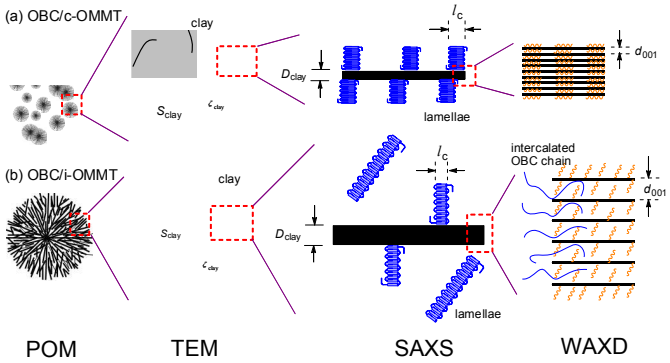

Scheme 1 Illustration of hierarchical structures for OBC/c-OMMT (a) and OBC/i-OMMT (b) at different scales.

3.6. Tensile Behavior. Since the hierarchical structures of OBC/c-OMMT and OBC/i-OMMT nanocomposites are quite different, the properties of the nanocomposites will be inevitably influenced. Fig. 8 shows the representative uniaxial stress-strain curves of the neat OBC and two types of nanocomposite with a clay loading of 1.0 and 3.0 wt% at room temperature. The mechanical data are summarized in Table 4. The nanocomposites exhibit similar stress-strain curves with typical characteristics of elastomers, i.e., diffused yielding point upon deformation, as compared to plastics. It is observed that for the neat OBC and OBC/c-OMMT samples, the stress increases steadily in the initial period of tensile drawing and strain-hardening occurs with a larger slope at the late stage. Moreover, the elastic modulus, yield stress and stress at break of the nanocomposites are always larger than those of the neat OBC (Table 4), implying that clay can enhance tensile strength of OBC, which is widely reported in the literatures.[62-64] This is due to that the clay layers can serve as the physically crosslinking points, thus stress can be efficiently transferred from polymer to the nanoclay and the chain slippage is reduced.

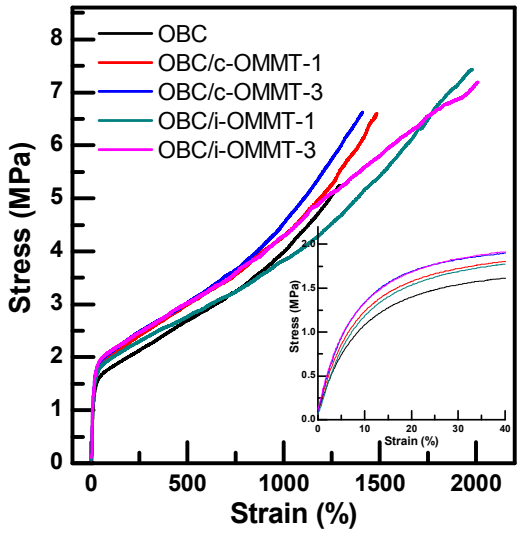

Fig. 8 Stress-strain curves of the neat OBC and selected OBC/c-OMMT and OBC/i-OMMT nanocomposites with a clay loading of 1.0 and 3.0 wt%. Inset shows the enlarged zone at small stains.

The tensile behaviors of OBC/c-OMMT and OBC/i-OMMT nanocomposites are also different to some extent. Firstly, the strain-hardening phenomenon in OBC/i-OMMT is not so pronounced as that in OBC/c-OMMT. Secondly, the OBC/i-OMMT nanocomposites exhibit a larger strain at break than the OBC/c-OMMT nanocomposites. These differences can be interpreted in terms of the different aggregation structures of OBC/c-OMMT and OBC/i-OMMT nanocomposites. As revealed by the values of Φ_s, more amorphous phase is located among the macroscopic crystals in OBC/i-OMMT, which mainly contributes to the elongation upon uniaxial tensile. Therefore, larger strain at break can be reached for OBC/i-OMMT nanocomposites. On the other hand, in OBC/c-OMMT more amorphous phase is included into inter-lamellae and the lamellar crystal thickness is larger as well, leading to the larger long periods of OBC/c-OMMT nanocomposites. As a result, for the same molecular weight of OBC, fewer tie molecules, which

Table 4 Tensile properties of the selected nanocomposites with a clay loading of 1.0 and 3.0 wt% and the neat OBC

Sample name	5% secant modulus (MPa)	Yield stress (MPa)	Stress at break (MPa)	Strain at break (%)
neat OBC	13.8±0.2	1.5±0.2	5.0±0.4	1290±30
OBC/c-OMMT-1	17.5±0.1	1.8±0.2	6.5±0.5	1490±30
OBC/c-OMMT-3	18.2±0.2	2.0±0.3	6.6±0.4	1410±50
OBC/i-OMMT-1	16.8±0.2	1.7±0.2	7.4±0.6	1980±60
OBC/i-OMMT-3	18.5±0.3	2.0±0.3	7.3±0.6	2010±80

span and connect different lamellar crystals and generally play a crucial role on the mechanical behavior,[65-67] are formed in OBC/c-OMMT, and the nanocomposites break at a smaller strain accordingly. The thicker lamellar crystals and less amorphous phase among the macroscopic crystals also result in more obvious strain-hardening behavior of the OBC/c-OMMT nanocomposites. It is also expected that such an aggregation structure of OBC/c-OMMT nanocomposites is advantageous to improvement of the impact property and related study is in progress.

Conclusions

Above results show that the OBC/c-OMMT and OBC/i-OMMT nanocomposites have different hierarchical structures. Firstly, the dispersion states of OMMT are different. In single c-OMMT particles, more clay layers are densely stacked, leading to a smaller size of the clay particles, larger distance between the adjacent clay particles and a smaller volume fraction of the clay particles. The nucleation ability of c-OMMT on crystallization of OBC is stronger than that of i-OMMT, as revealed by the higher crystallization temperature and smaller crystallites in the OBC/c-OMMT nanocomposites. Both the thicknesses of the lamellar crystal and the amorphous layer in OBC/c-OMMT are larger than those in OBC/i-OMMT, resulting in a larger long period. There is more amorphous phase included into the inter-lamellae but less amorphous phase located among the macroscopic crystals in OBC/c-OMMT. The OBC/c-OMMT and OBC/i-OMMT nanocomposites also exhibit different tensile behaviors, such as more obvious strain-hardening behavior and smaller strain at break for the OBC/c-OMMT nanocomposites, which originate from their different hierarchical structures.

Acknowledgements

This work was supported by the National Basic Research Program of China (973 Program) (2011CB606005) and the National Natural Science Foundation of China (51073138). The authors would also like to thank beamlines BL16B1 and BL14B1 (Shanghai Synchrotron Radiation Facility) for providing the beam time. The OBC samples were kindly supplied by Dow Chemical Company.

References

1 D. J. Arriola, E. M. Carnahan, P. D. Hustad, R. L. Kuhlman and T. T. Wenzel, *Science*, 2006, **312,** 714-719.
2 P. S. Chum and K. W. Swogger, *Prog. Polym. Sci.*, 2008, **33,** 797-819.
3 D. U. Khariwala, A. Taha, S. P. Chum, A. Hiltner and E. Baer, *Polymer*, 2008, **49,** 1365-1375.
4 H. P. Wang, D. U. Khariwala, W. Cheung, S. P. Chum, A. Hiltner and E. Baer, *Macromolecules*, 2007, **40,** 2852-2862.
5 P. Dias, Y. J. Lin, B. Poon, H. Y. Chen, A. Hiltner and E. Baer, *Polymer*, 2008, **49,** 2937-2946.
6 A. R. Kamdar, H. P. Wang, D. U. Khariwala, A. Taha, A. Hiltner and E. Baer, *J. Polym. Sci., Part B: Polym. Phys.*, 2009, **47,** 1554-1572.
7 J. Jin, J. A. Du, Q. H. Xia, Y. R. Liang and C. C. Han, *Macromolecules*, 2010, **43,** 10554-10559.
8 H. E. Park, J. M. Dealy, G. R. Marchand, J. A. Wang, S. Li and R. A. Register, *Macromolecules*, 2010, **43,** 6789-6799.
9 F. Zuo, C. Burger, X. M. Chen, Y. M. Mao, B. S. Hsiao, H. Y. Chen, G. R. Marchand, S. Y. Lai and D. Chiu, *Macromolecules*, 2010, **43,** 1922-1929.
10 J. Jin, J. Du, H. Y. Chen and C. C. Han, *Polymer*, 2011, **52,** 6161-6172.
11 J. Jin, C. Z. Zhao, J. Du and C. C. Han, *Macromolecules*, 2011, **44,** 4326-4334.
12 G. M. Liu, Y. Guan, T. Wen, X. W. Wang, X. Q. Zhang, D. J. Wang, X. H. Li, J. Loos, H. Y. Chen, K. Walton and G. Marchand, *Polymer*, 2011, **52,** 5221-5230.
13 F. Zuo, Y. M. Mao, X. W. Li, C. Burger, B. S. Hsiao, H. Y. Chen and G. R. Marchand, *Macromolecules*, 2011, **44,** 3670-3673.
14 S. Li, R. A. Register, J. D. Weinhold and B. G. Landes, *Macromolecules*, 2012, **45,** 5773-5781.
15 T. Wen, G. Liu, Y. Zhou, X. Zhang, F. Wang, H. Chen, J. Loos and D. Wang, *Macromolecules*, 2012, **45,** 5979-5985.
16 T. Wen, Y. Zhou, G. M. Liu, F. S. Wang, X. G. Zhang, D. J. Wang, H. Y. Chen, K. Walton, G. Marchand and J. Loos, *Polymer*, 2012, **53,** 529-535.
17 Z. Z. Tong, J. Huang, B. Zhou, J. T. Xu and Z. Q. Fan, *Macromol. Chem. Phys.*, 2013, **214,** 605-616.
18 Z. Z. Tong, J. T. Xu, S. J. Xia and Z. Q. Fan, *Polym. Int.*, 2013, **62,** 228-237.
19 X. Zhou, J. Feng, D. Cheng, J. Yi and L. Wang, *Polymer*, 2013, **54,** 4719-4727.
20 Z. Z. Tong, B. Zhou, J. Huang, J. T. Xu and Z. Q. Fan, *Macromolecules*, 2014, **47,** 333-346.
21 T. G. Gopakumar, J. A. Lee, M. Kontopoulou and J. S. Parent, *Polymer*, 2002, **43,** 5483-5491.
22 S. S. Ray and M. Okamoto, *Macromol. Rapid Commun.*, 2003, **24,** 815-840.
23 S. S. Ray and M. Okamoto, *Prog. Polym. Sci.*, 2003, **28,** 1539-1641.
24 A. Usuki, N. Hasegawa and M. Kato, *Adv. Polym. Sci.*, 2005, **179,** 135-195.
25 M. W. Spencer, D. L. Hunter, B. W. Knesek and D. R. Paul, *Polymer*, 2011, **52,** 5369-5377.
26 C. Chen and D. G. Baird, *Polymer*, 2012, **53,** 4178-4186.
27 M. Alexandre and P. Dubois, *Mater. Sci. Eng. R: Rep.*, 2000, **28,** 1-63.
28 X. Kornmann, H. Lindberg and L. A. Berglund, *Polymer*, 2001, **42,** 1303-1310.

29 X. Zhang and L. S. Loo, *J. Polym. Sci., Part B: Polym. Phys.*, 2008, **46,** 2605-2617.
30 X. Zhang and L. S. Loo, *Macromolecules*, 2009, **42,** 5196-5207.
31 D. Shah, P. Maiti, E. Gunn, D. F. Schmidt, D. D. Jiang, C. A. Batt and E. P. Giannelis, *Adv. Mater.*, 2004, **16,** 1173-1177.
32 L. Qiu, W. Chen and B. Qu, *Polymer*, 2006, **47,** 922-930.
33 Y. Yoo, L. Cui, P. J. Yoon and D. R. Paul, *Macromolecules*, 2010, **43,** 615-624.
34 S. P. Liu and L. C. Tu, *International Communications in Heat and Mass Transfer*, 2011, **38,** 879-886.
35 A. F. Osman, G. A. Edwards, T. L. Schiller, Y. Andriani, K. S. Jack, I. C. Morrow, P. J. Halley and D. J. Martin, *Macromolecules*, 2012, **45,** 198-210.
36 J. T. Xu, Y. Q. Zhao, Q. Wang and Z. Q. Fan, *Polymer*, 2005, **46,** 11978-11985.
37 J. T. Xu, Y. Q. Zhao, Q. Wang and Z. Q. Fan, *Macromol. Rapid Commun.*, 2005, **26,** 620-625.
38 Z. Z. Tong, B. Zhou, J. Huang, J. T. Xu and Z. Q. Fan, *Compos. Sci. Technol.*, 2013, **85,** 111-117.
39 J. T. Yoon, W. H. Jo, M. S. Lee and M. B. Ko, *Polymer*, 2001, **42,** 329-336.
40 P. J. Yoon, D. L. Hunter and D. R. Paul, *Polymer*, 2003, **44,** 5323-5339.
41 S. Hotta and D. R. Paul, *Polymer*, 2004, **45,** 7639-7654.
42 B. D. Cullity, *"Elements of X-ray diffraction", 2nd ed.* Addison-Wesley, Reading: 1978.
43 F. Perrin-Sarazin, M. T. Ton-That, M. N. Bureau and J. Denault, *Polymer*, 2005, **46,** 11624-11634.
44 C. G. Vonk and G. Kortleve, *Kolloid Z. Z. Polym.*, 1967, **220,** 19.
45 G. R. Strobl and M. J. Schneider, *J. Polym. Sci., Part B: Polym. Phys.*, 1980, **18,** 1343-1359.
46 G. R. Strobl, M. J. Schneider and I. G. Voigt-Martin, *J. Polym. Sci., Part B: Polym. Phys.*, 1980, **18,** 1361-1381.
47 H. L. Chen, S. F. Wang and T. L. Lin, *Macromolecules*, 1998, **31,** 8924-8930.
48 H. J. Chiu, H. L. Chen, T. L. Lin and J. S. Lin, *Macromolecules*, 1999, **32,** 4969-4974.
49 B. Zhou, W. N. He, X. Y. Jiang, Z. Z. Tong, J.-T. Xu and Z.-Q. Fan, *Compos. Sci. Technol.*, 2014, **93,** 23-29.
50 B. Zhou, Z. Z. Tong, J. Huang, J. T. Xu and Z. Q. Fan, *CrystEngComm*, 2013, **15,** 7824-7832.
51 E. Di Maio, S. Iannace, L. Sorrentino and L. Nicolais, *Polymer*, 2004, **45,** 8893-8900.
52 A. Somwangthanaroj, E. C. Lee and M. J. Solomon, *Macromolecules*, 2003, **36,** 2333-2342.
53 J. T. Xu, Q. Wang and Z. Q. Fan, *Eur. Polym. J.*, 2005, **41,** 3011-3017.
54 B. Wunderlich, *Macromolecular Physics, Vol. 3, Crystal Melting*. Academic Press: New York, 1980.
55 G. Jimenez, N. Ogata, H. Kawai and T. Ogihara, *J. Appl. Polym. Sci.*, 1997, **64,** 2211-2220.
56 G. M. Kim, D. H. Lee, B. Hoffmann, J. Kressler and G. Stöppelmann, *Polymer*, 2001, **42,** 1095-1100.
57 D. M. Lincoln, R. A. Vaia, Z.-G. Wang, B. S. Hsiao and R. Krishnamoorti, *Polymer*, 2001, **42,** 09975-09985.
58 P. Maiti and M. Okamoto, *Macromol. Mater. Eng.*, 2003, **288,** 440-445.
59 C. Y. Ren, Z. Y. Jiang, X. H. Du, Y. F. Men and T. Tang, *J. Phys. Chem. B*, 2009, **113,** 14118-14127.
60 J. I. Weon, Z. Y. Xia and H. J. Sue, *J. Polym. Sci., Part B: Polym. Phys.*, 2005, **43,** 3555-3566.
61 K. E. Strawhecker and E. Manias, *Macromolecules*, 2001, **34,** 8475-8482.
62 F. M. Uhl, S. P. Davuluri, S. C. Wong and D. C. Webster, *Chem. Mater.*, 2004, **16,** 1135-1142.
63 K. Haraguchi, H. J. Li, H. Y. Ren and M. F. Zhu, *Macromolecules*, 2010, **43,** 9848-9853.
64 C. J. Wu, A. K. Gaharwar, B. K. Chan and G. Schmidt, *Macromolecules*, 2011, **44,** 8215-8224.
65 K. H. Nitta and M. Takayanagi, *J. Polym. Sci., Part B: Polym. Phys.*, 1999, **37,** 357-368.
66 J. J. Janimak and G. C. Stevens, *J. Mater. Sci.*, 2001, **36,** 1879-1884.
67 A. Makke, O. Lame, M. Perez and J. L. Barrat, *Macromolecules*, 2012, **45,** 8445-8452.

Table of Contents Entry

Hierarchical Structures of Olefinic Blocky Copolymer/Montmorillonite Nanocomposites with Collapsed and Intercalated Clay Layers

Zai-Zai Tong, Bing Zhou, Jie Huang, Jun-Ting Xu,* Zhi-Qiang Fan

MOE Key Laboratory of Macromolecular Synthesis and Functionalization, Department of Polymer Science & Engineering, Zhejiang University, Hangzhou 310027, China

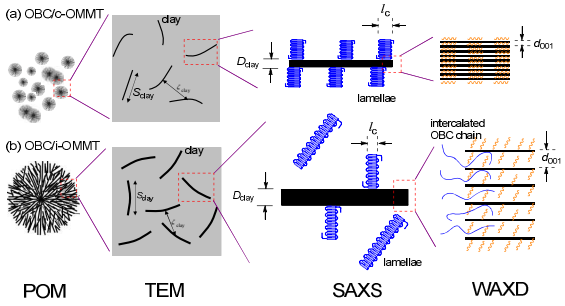

Hierarchical Structures of two types of nanocomposite at different scales were characterized with various techniques.